Physical Modeling Investigation On Failure Mechanism of Layered Surrounding Rock And Deformation Characteristics Based On Digital Speckle Correlation Method

Zhenlong Zhao
China University of Mining and Technology State Key Laboratory for Geomechanics and Deep Underground Engineering

Hongwen Jing (hongwenjingcumt@163.com)
China University of Mining and Technology State Key Laboratory for Geomechanics and Deep Underground Engineering https://orcid.org/0000-0003-0363-970X

Li Zhang
China University of Mining and Technology

Xinshuai Shi
China University of Mining and Technology State Key Laboratory for Geomechanics and Deep Underground Engineering

Research Article

Keywords: symmetrical physical model, layered rock mass, supporting structure, deformation characteristic, failure mechanism, digital speckle correlation method

Posted Date: July 20th, 2021

DOI: https://doi.org/10.21203/rs.3.rs-654998/v1

Physical modeling investigation on failure mechanism of layered surrounding rock and deformation characteristics based on digital speckle correlation method

Zhenlong Zhao[1], Hongwen Jing[1,*], Li Zhang[1] and Xinshuai Shi[1,2]

[1] State Key Laboratory for Geomechanics and Deep Underground Engineering, China University of Mining and Technology, Xuzhou 221116, PR China
[2] Graduate School of Engineering, Nagasaki University, 1-14 Bunkyo, Nagasaki 852-8521, Japan
*Correspondence: hongwenjingcumt@163.com (H.J.)

Abstract: In rock mass engineering such as underground coal mine roadway, underground tunnel and water conservancy and hydropower chamber construction, layered rock mass is a type of surrounding rock mass that is often encountered. Due to the influence of bedding structural plane, its deformation process and failure mode are obviously different from that of intact enclosed rock mass. For the layered rock structure of roadway, the previous studies mainly focused on the situation of no support or single bolt support, but there is still a lack of experimental studies on the mechanical properties and failure laws of surrounding rock under different support methods. In this paper, the deep roadway and surrounding rock environment with a buried depth of 742-877m are taken as the engineering background, which is located in Anhui Province, China. Based on the similarity theorem and similarity criterion, river sand is used as aggregate, gypsum and cement are used as cementing material. According to the test results, 5:0.7:0.3, 6:0.3:0.7 and 4:0.5:0.5 of river sand, gypsum and cement were selected as the similar materials to simulate the surrounding rock of the roadway, and the bedding plane structure of the surrounding rock of the roof and floor near the roadway was designed by using the self-developed similar material physical model test bed. Digital Speckle Correlation Method (DSCM) is used to analyze the deformation evolution process of roadway surrounding rock under three supporting schemes: no-support scheme, bolt support scheme, and synergistic support of bolt and anchor cable. Based on this, the failure mode and instability mechanism of deep layered surrounding rock are further discussed. The results show that the tensile and shear resistance of laminated roof surrounding rock is weak, and the laminated roof is easily separated from each other at the bedding plane without support, resulting in bending deformation and bed separation. After adopting effective support, the laminated roof surrounding rock is transformed into a composite beam bearing structure, and the stability of surrounding rock increases. The research results have certain theoretical guiding significance and engineering application value for practical engineering.

Keywords: symmetrical physical model; layered rock mass; supporting structure; deformation characteristic; failure mechanism; digital speckle correlation method

1. Introduction

The layered rock mass is a kind of rock mass often encountered in underground rock mass engineering, such as underground coal mine roadway, underground tunnel and water conservancy and hydropower chamber construction as shown in **Fig.1 (Lyu et al., 2019; Do et al., 2019; Bewick et al., 2019)**. Under the influence of bedding structural plane, the deformation and strength of the rock mass have obvious anisotropy, and the failure characteristics of the rock mass are obviously different from that of the intact rock mass. In addition, in deep rock engineering, the surrounding rock environment is mostly sedimentary rock, and most of the sedimentary rocks are mainly distributed in layers. In deep special environment, the deformation and stability control of surrounding rock in excavation space are more prominent. As the excavation of roadway itself is a unloading process, the stress redistribution caused by it will make the

surrounding rock in a worse stress environment, leading to the existence of cracks and joints in the surrounding rock continuously through and expand, resulting in new fissures, and finally lead to roadway failure and caving, leading to engineering accidents **(Feng et al., 2017)**. Different layered rock masses have different layered structures and bedding planes, which leads to more complex deformation and failure characteristics of deep layered rock masses with high stress than that of intact rock masses **(Ding et al., 2019)**. Therefore, it is of great significance to study the stability of roadway by the structural effect of engineering surrounding rock.

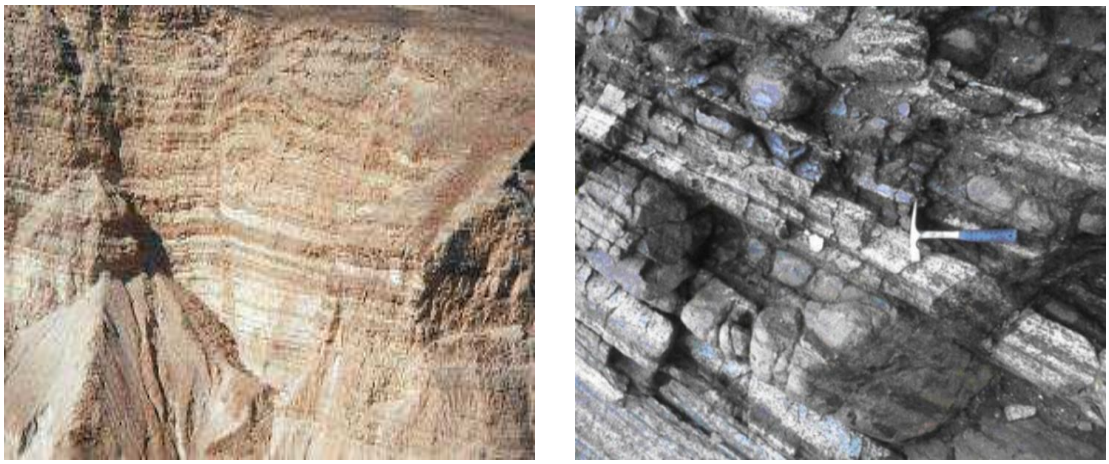

Figure 1. Layered rock masses in nature.

In the study of layered surrounding rock roadway, scholars from the theory, numerical, physical model and other aspects of a large number of studies **(Lyu et al.,2020; Zhou et al., 2020; Xu et al., 2017; Halakatevakis and Sofianos 2010; Zhou et al., 2017)**. However, in the study of the stability of underground engineering rock mass, as a result of theoretical analysis and field monitoring methods reflect the characteristics of the stability control of deep surrounding rock and its deformation and failure of the effect is not very ideal, different surrounding rock conditions and engineering factors such as time, location, affects the deformation of deep roadway damage as a result, the similar material model test is based on the similarity theory, As an important means to study the roadway support and surrounding rock deformation, it can directly reflect the deformation and failure characteristics of roadway surrounding rock under different support conditions and the related physical phenomena, and compare the test results. It can verify each other with the numerical simulation results and supplement them on the basis of this, and give a clear conclusion. Compared to similar material model test prototype test, in time, space and cost has dropped significantly, and have difficulty making model low, save time and effort, and the advantages of convenient, easy to analyze, in addition, the original rock of roadway affected by various factors, and can change a similar model test influencing factors and study its influence on surrounding rock of roadway, repeatability, It has a certain guiding function to the actual engineering application.

Existing deep roadway physical test, however, most of the surrounding rock is simplified to a complete rock mass, and the study of bedded surrounding rock of roadway is less, and the layered rock mass affected by internal bedding, joint, has obvious anisotropy characteristic, of deep roadway deformation and failure mechanism of layered rock mass and lack of system of further research **(Yang et al., 2015; Yoshinaka et al., 2008; Asadi et al., 2013; Zhao et al., 2020)**. In addition, for a long time, the deformation of deep roadway has always been the target of the study on the stability control of surrounding rock. Many experts and scholars have developed a variety of support technologies around the deformation control of surrounding rock. Especially with the development of science and technology, all kinds of monitoring equipment are used in the study of physical models. From the view of engineering practice, the

control effect of these techniques on the large deformation of deep roadway surrounding rock is not very significant.

To sum up, although relevant scholars have carried out fruitful studies on the stability of layered surrounding rock mass in roadway, the understanding of deformation and failure mechanism of layered surrounding rock mass in deep layered surrounding rock mass still needs to be further studied due to the complexity of stress environment and the particularity of rock bedding structural plane. In particular, there are few research results on deformation characteristics and failure mechanism of surrounding rock under different supporting modes of layered rock roadway. In this paper, therefore, in eastern China, the engineering background of a deep roadway and surrounding rock conditions, in deep rock and soil mechanics in China university of mining and underground engineering state key laboratory of underground engineering is based on physical model test system, according to the loading before excavation way of instability and failure of deep roadway from excavation to the whole process of the research, With the help of digital speckle technique, the deformation characteristics and failure mechanism of layered surrounding rock in deep rectangular roadway under three kinds of support methods are deeply discussed.

2. Methodology

2.1. Testing system

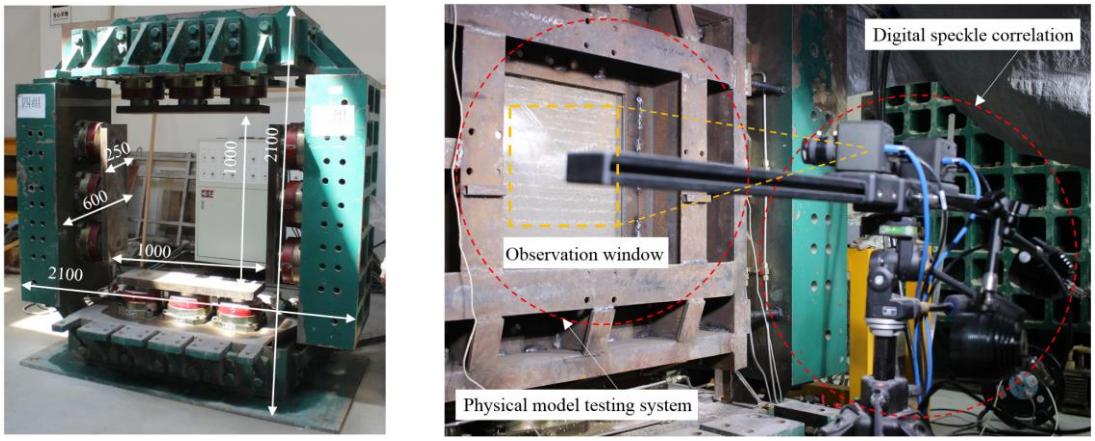

(a) Loading system (b) Monitoring system

Figure 2. Testing system.

A self-developed two-dimensional model testing system for underground rock mass engineering is used to carry out physical modeling investigation. It includes the loading system, hydraulic servo system and computer control system. The maximum model size allowed to be loaded by the loading system is 1000 mm (height) × 1000 mm (length) × 250 mm (width) in **Fig. 2**. The hydraulic system and computer control system can realize the independent control of the loading system in the four directions of loading of top, bottom, left and right. The loading unit in each direction are controlled synchronously by three hydraulic cylinders to ensure the uniform force of the physical model. In order to monitor deformation process of surrounding rock in real-time, a transparent acrylic plate with a thickness of 30 mm is fixed to the front of the model to apply displacement-constrained boundary condition. Similarly, a steel plate is fixed to the back of the model, and a detachable baffle is reserved at the roadway location and its size is the same as the roadway size to facilitate tunnel excavation. The maximum load that each loading unit can load is 300 kN, the stroke is 50 mm and the control precision is ±0.5 %.

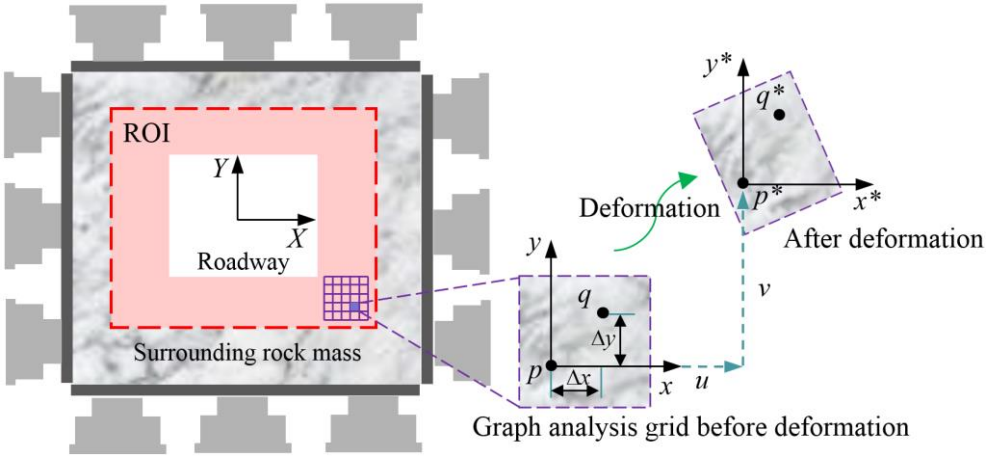

Figure 3. Schematic diagram of digital speckle correlation method.

Digital Speckle Correlation Method (DSCM) is a kind of deformation measurement method based on Digital Image Correlation (DIC) (**Amodio et al., 2003; Bruckat al., 1989; Yang et al., 2020; Li et al., 2019**). Its basic principle is to track the movement of geometric points on the model surface by image matching before and after deformation to obtain displacement field. DSCM can replace the traditional displacement sensor, not only can complete the displacement sensor can not achieve the deformation measurement, but also can quickly realize the deformation measurement, so DSCM in the field of rock mechanics is receiving more and more attention. So in this study, DSCM was used to monitor the deformation process of roadway surrounding rock.

In the application process of DSCM, in order to improve the calculation efficiency and accuracy, only the region of interest (ROI) on the model is selected for calculation when selecting the speckle region. The ROI and calculation principle are shown in **Fig. 3**. Firstly, the camera system is used to obtain the image before and after the deformation of the object surface. Through the digital image correlation algorithm, the matching degree of the image before and after the deformation is calculated, so as to determine the corresponding geometric points before and after the deformation of the object and compare, match and calculate, then the displacement of the whole area can be obtained

The correlation coefficient formula is：

$$COF = \frac{\sum_{i=1}^{m}\sum_{j=1}^{m}\left[f\left(x_i, y_i\right)-\overline{f}\right]\cdot\left[g\left(x_i^*, y_j^*\right)-\overline{g}\right]}{\sqrt{\sum_{i=1}^{m}\sum_{j=1}^{m}\left[f\left(x_i, y_i\right)-\overline{f}\right]^2\cdot\sum_{i=1}^{m}\sum_{j=1}^{m}\left[g\left(x_i^*, y_j^*\right)-\overline{g}\right]^2}} \tag{1}$$

where *f(x, y)* and *g(x∗, y∗)* are respectively the gray values of the reference points before and after deformation, F and g are the average gray values of the subsets before and after deformation. When the correlation coefficient is 1, it means that the two subsets are completely correlated. When the correlation coefficient is 0, it means that the two subsets are completely unrelated. Assume that the coordinate systems *(x, y)* and *(x*, y*)* are respectively the same point in the pixel subsets of the sample monitoring surface, namely, the coordinate systems of *P* point before deformation and *P** point after deformation.

The correlation function of the two coordinate systems before and after deformation:

$$\left.\begin{aligned} x^* &= x+\mu+\frac{\partial\mu}{\partial x}\Delta x+\frac{\partial\mu}{\partial y}\Delta y \\ y^* &= y+\nu+\frac{\partial\nu}{\partial x}\Delta x+\frac{\partial\nu}{\partial y}\Delta y \end{aligned}\right\} \tag{2}$$

where μ, ν, $\frac{\partial\mu}{\partial x}$, $\frac{\partial\mu}{\partial y}$, $\frac{\partial\nu}{\partial x}$, $\frac{\partial\nu}{\partial y}$ all are deformation parameters, μ, ν are horizontal and vertical relative displacement in coordinate system. After the test, the obtained image data was imported into the computer analysis system, and then the strain field evolution cloud map of the surrounding rock surface of the roadway during the test was obtained.

2.2. Experimental preparation

This study takes the deep roadway of 742-877 m buried depth as the engineering background, which is located in Anhui Province, China. The cross section of the roadway is horseshoe shape with a cross section size of 5100 × 4200 mm. The rock strata of the roof and floor are mainly siltstone, fine sandstone and mudstone, and their physical and mechanical parameters are shown in Fig. 1a and Table 2. Considering that the height of the physical model is 1000mm and the rock strata of the roof and floor of the original roadway, the upper and lower distances of 15m are taken from the center of the original roadway, and the geometric similarity ratio is determined as 33.3. The size of the roadway is 170 × 140 mm, and it is located in the middle of the physical model. The upper, lower, left and right sides of the model and roadway are symmetry.

Table 1 Mechanical parameters of similar model. A is the prototype value, B is the theoretical value , C is the actual value.

Lithology	Thickness (mm)			UCS (MPa)			Elastic modulus (MPa)		
	A	B	C	A	B	C	A	B	C
Mudstone	1800	54	60	21.3	0.51	0.55	2.22	52.9	56
Fine sandstone	4900	147	165	77.6	1.85	1.68	8.34	198.6	203
siltstone	9600	279	320	45.4	1.08	1.07	6.44	153.3	159
Fine sandstone	12200	366	405	74.5	1.77	1.68	8.57	204.0	203
Mudstone	1500	45	50	22.4	0.53	0.55	2.38	56.7	56

The suitable similar materials play a key role in the physical model experiments. The surrounding rock of deep roadway is in a high stress environment, and there are obvious ductile deformation characteristics after the peak deformation. So the basic mechanical tests of similar materials with different ratios are carried out based on the compressive strength and elastic modulus, and the most appropriate ratio is selected for the physical model test.

To obtain the appropriate material ratio matching the physical and mechanical properties of the original siltstone in the engineering site, the similarity ratio should be determined according to the similarity criterion in **Eq. (3)**.

$$\left.\begin{aligned} C_\sigma &= C_\gamma C_L \\ C_\sigma &= C_\varepsilon C_E \end{aligned}\right\} \tag{3}$$

where C_σ is the stress similarity ratio, C_γ is the bulk weight similarity ratio, C_L is the geometric

similarity ratio, C_E is the elastic modulus similarity ratio, C_ε is the strain similarity ratio and $C_\varepsilon = 1$ in this paper.

In this experiment, the simulated rock strata are mainly sedimentary rocks, and most of the sedimentary rocks are composed of mineral particles aggregated together. So the similar materials mixed by aggregate and cementing materials are used to simulate the surrounding rock of roadway. In similar materials commonly used aggregate materials are quartz sand, aluminum powder, iron powder, and commonly used cementing materials include cement, calcium carbonate, paraffin, gypsum and so on. Based on the existing research results, the well graded quartz sand are selected as aggregate, cement and gypsum as cement. The mass ratio of aggregate to cementitious material is the basis for grouping similar material specimens, in which the mass ratio of aggregate to cementing material was 3:1, 4:1, 5:1 and 6:1 respectively. Under the condition of keeping the mass ratio of aggregate to cementitious material unchanged, the mass ratio of gypsum to cement is changed to 3:7, 5:5 and 7:3 respectively. A total of 12 groups of similar material specimens with different ratios of quartz sand, gypsum and cement are obtained, in which water accounted for 20% of the total weight of quartz sand, gypsum and cement. It was determined that the bulk density of similar materials with different proportions was about 17.6-18.4 kN /m^3. Considering the simplification of the physical model, 25kN/m3 was taken as the average weight of overlying strata of the prototype roadway, so the bulk density similarity ratio was 3.6-4.6. For convenience of calculation, the bulk density similarity ratio was determined as 4. Therefore, according to **Eq. (3)**, the strength similarity ratio and elastic modulus similarity ratio are both 42. After calculation, the mechanical parameters of lithology of each layer in the model can be obtained as shown in **Table 1**.

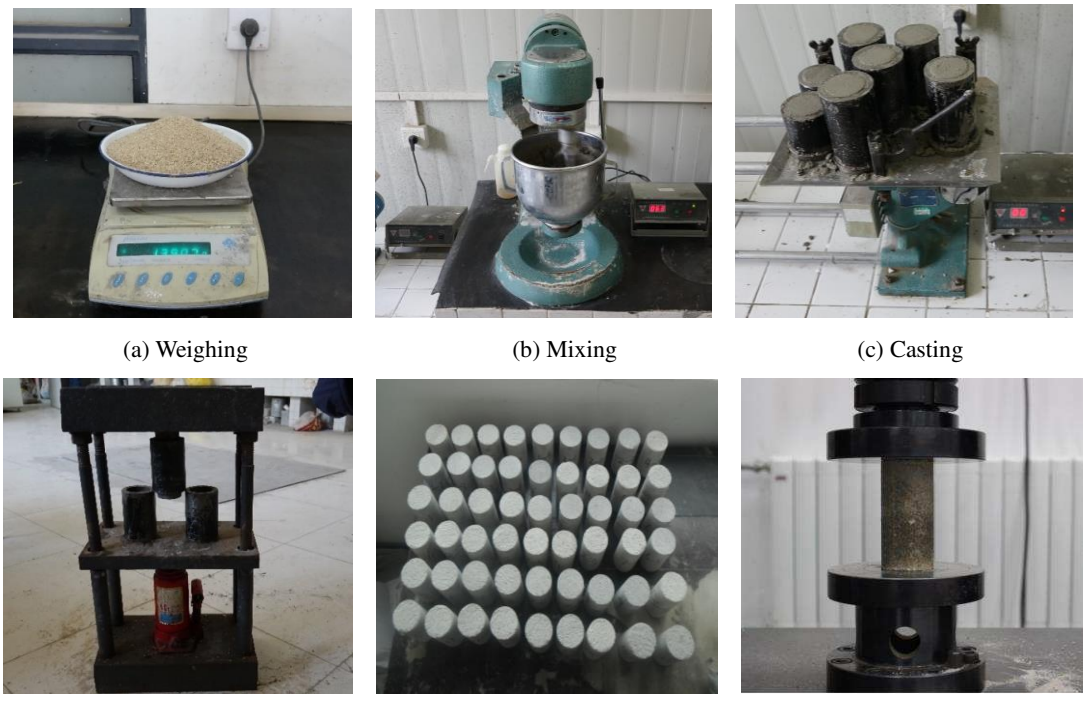

(a) Weighing (b) Mixing (c) Casting

(d) Demoulding (e) Drying (f) Testing

Figure 4. Preparation of similar material specimens.

The standard cylinder specimens with the size of Φ 50mm×100mm were prepared according to the above mass ratio of similar materials, and deformation and failure characteristics of specimens were measured by using high-precision servo testing machine produced by MTS Company in the United States.

The preparation of similar material specimens includes weighing, mixing, vibrating, demoulding and drying, as shown in **Fig. 4**. Before the specimen preparation, to facilitate demoulding, release agent is evenly applied to the inner wall of the mold. In the preparation process, the similar materials are fully stirred and compacted in the mold. After the sample preparation is completed, the mold is removed 24 hours later, and then the specimen is placed in a ventilated room to dry naturally for 72 hours.

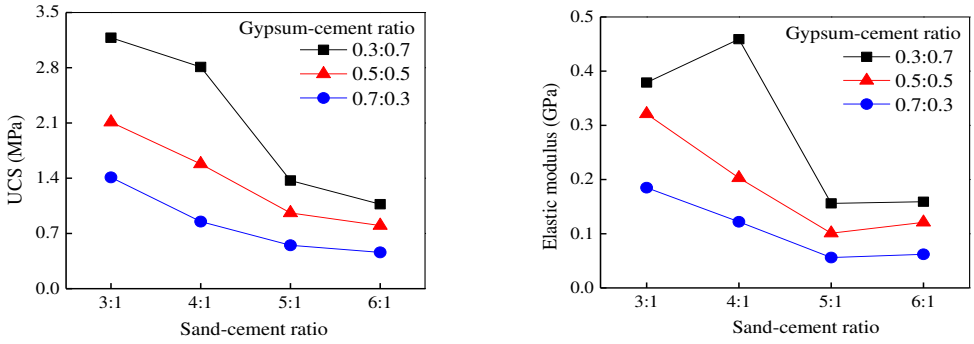

Figure 5. Uniaxial compressive strength and elasticity modulus of similar materials.

Figure 5 gives the uniaxial compressive strength and elastic modulus of similar material specimens with different proportions. Compared with the theoretical value of similar material required in **Table 1**, the similar materials with the mass ratios of quartz sand, gypsum and cement of 5:0.7:0.3, 6:0.3:0.7 and 4:0.5:0.5 are selected to simulate the mudstone, siltstone and fine sandstone in the surrounding rock of roadway. It can be seen from **Fig. 6a** that the stress-strain curves of similar material specimens cemented by quartz sand, gypsum and cement have obvious five stages: initial compaction, linear elastic, plastic strengthening, post-peak softening and residual strength. It can be seen from **Fig. 6b** that the failure modes are mainly splitting and shearing. Because the failure characteristics and stress-strain curves of similar material specimens are similar to those of rocks, it is feasible to simulate the underground surrounding rock with similar material determined by the selected similarity ratio. In addition, the bedding is simulated by 40 mesh mica powder, the fine iron wire with a length of 83mm and a diameter of 0.73mm was selected as the similar material of the anchor rod, and the fine iron wire with a length of 206mm and a diameter of 0.73mm was selected as the similar material of the anchor cable.

(a) Stress-strain curves (b) Failure modes

Figure 6. Stress-strain curves and failure modes of similar materials in uniaxial compression test.

2.3. Experimental process

In this study, three kinds of supporting schemes of roadway surrounding rock are designed, which are no support, bolt support, combined support of bolt and anchor cable, and the rockbolts were embedded and fixed according to the specified position in the preparing process of the model.

Parameter and layout of anchor bolt and anchor cable in roadway section are shown in **Fig. 7**. Row spacing of both anchor bolt and anchor cable in the thickness direction is 25mm. The layer thickness of the surrounding rock near the roadway is 30mm, and the actual thin layer thickness with a thickness of 0.9m is simulated. With the roadway as the center, 10 bedding planes are arranged within 300mm of the roof and floor of the roadway. The specific physical model design is shown in **Fig. 8**.

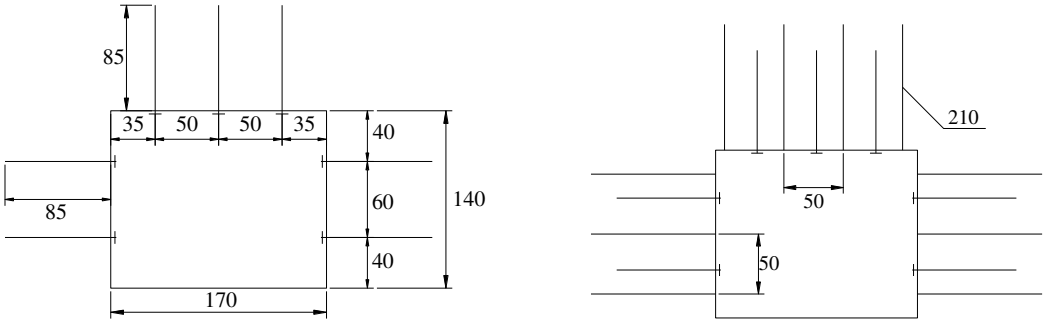

(a) Bolt support (b) Joint support of bolt and anchor cable

Figure 7. Supporting scheme.

The buried depth of the origin roadway is 742m-877m, the buried depth of the prototype roadway is 742m-877m, the vertical stress is determined by the weight of the overlying strata, and the lateral stress coefficient is 1.2. Therefore, the vertical stress and horizontal stress of the origin roadway can be calculated to be 18.6-21.9 MPa and 22.3-26.3 MPa respectively. Considering the stress similarity ratio, the vertical stress and horizontal stress applied to the physical model are 18.6-21.9 MPa and 18.6-21.9 MPa respectively. The boundary conditions of the model test were considered according to the most unfavorable conditions, the maximum vertical stress was 21.9MPa, and the maximum horizontal stress was 26.3MPa. According to the interaction area between the loading unit of the testing machine and the physical model, the horizontal force Fx and vertical force Fy that need to be applied to the physical model are calculated to be 117.00kN and 141.75kN respectively.

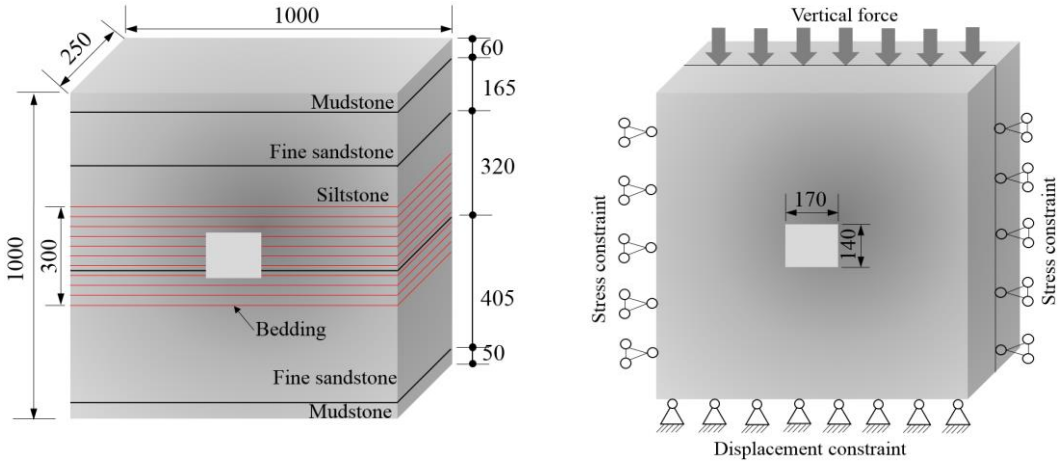

(a) Physical model design (b) Boundary conditions

Figure 8. Schematic diagram of physical model.

Compared with the actual excavation process of underground engineering, the loading mode of the testing system is more reasonable. In order to truly restore the stress process of the surrounding rock of underground roadway, the loading process of the model can be summarized as first loading the surrounding rock to the prestress in the vertical and horizontal directions, then excavating the roadway, then keeping the

horizontal direction stable, and loading the model in the vertical direction until the sample is destroyed.This testing system adopts the method of the loading first and then excavation. Firstly, the upper, lower, left and right boundaries of the physical model were loaded to the designed stress. For 30 minutes, after the stress has been fully transferred inside the physical model, then the roadway was excavated after the stress state of rock mass reached the initial stress equilibrium. In the process of roadway excavation, the stress evolutions of surrounding rock mass were monitored in real time. Therefore, stress boundary conditions are presented before roadway excavation, stress boundary conditions are presented on both sides and displacement boundary conditions are presented at the bottom after roadway excavation, and boundary conditions of roof loading model are shown in Fig. 2a and 2b respectively.

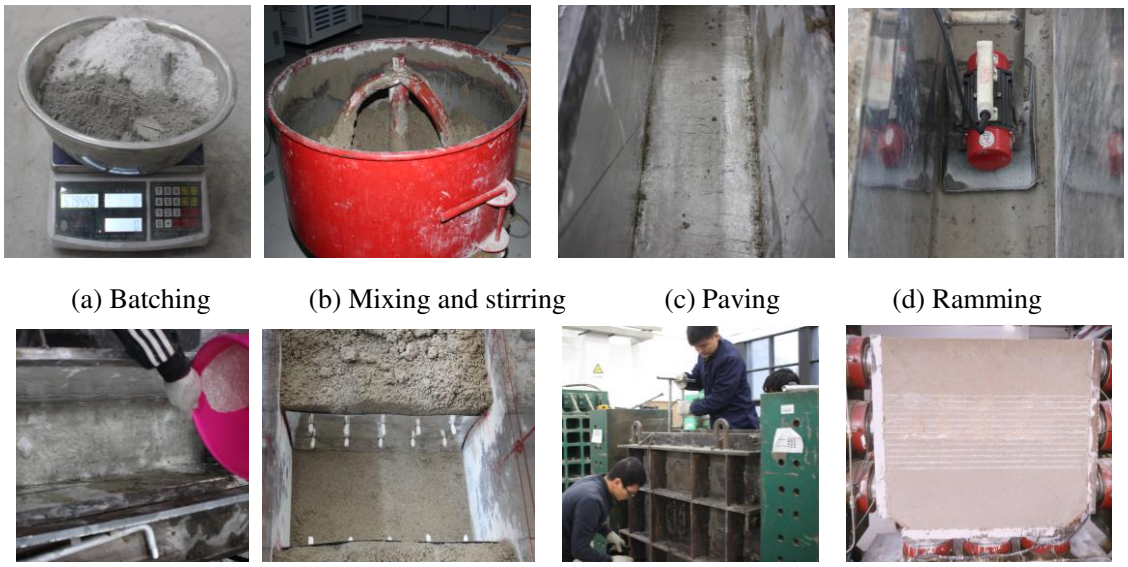

(a) Batching (b) Mixing and stirring (c) Paving (d) Ramming

(e) Laying bedding (f) Embedding support (g) Capping (h) Demoulding and drying

Figure 9. Preparation process of physical model.

The experimental process is mainly divided into two parts: model preparation and stress loading.

The size of the model in this test is 1000 mm × 1000 m × 250 m. According to the surrounding rock conditions in the engineering field, different rock layers are paved with similar materials of different proportions. The model making process mainly includes batching, mixing, paving, vibrating, laying bedding surface, embedding anchor rod and anchor cable, top compaction and demoulding, as shown in **Figure 7**. Before installing the front and rear baffles of the model, the positioning paper is put on the baffles to facilitate the determination of the layering position of the model and roadway position. Before paving each layer, the amount of river sand, gypsum and cement should be calculated in advance, and poured into the mixer to mix evenly, so that one layer is paved before the next layer is prepared. Pour the evenly stirred material into the model frame and spread it flat. After being vibrated with a hammer, the material is compacted by a vibrating machine. When using mica powder to lay the bedding surface, the powder should be evenly scattered and the dosage should be paid attention to. About 24 hours after the completion of the model pouring, the front and back baffles of the model frame were removed, and the model was left for 72 hours to be air-dried under natural conditions. After the completion of the model preparation, initial horizontal and vertical in-situ stresses are applied to the model first, and then vertical loads are continuously applied by controlling the top indenter. The digital speckle system is used to monitor the deformation and failure of surrounding rock in the process of roof loading.

3. Results and analysis

3.1. Deformation characteristic

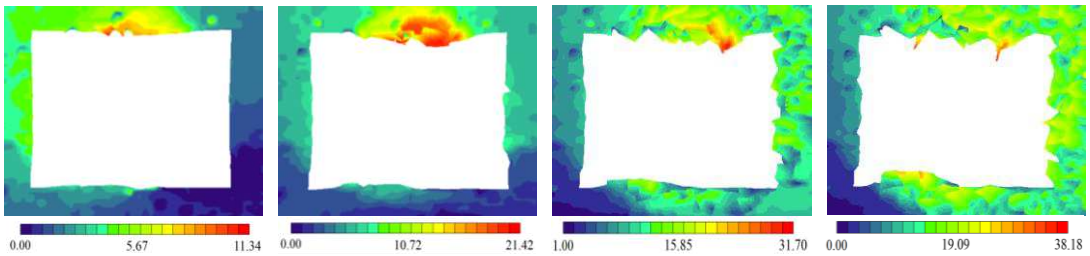

(a) 2200s (b) 7000s (c) 7800s (d) 9000s

Figure 10. Displacement field in scheme one.

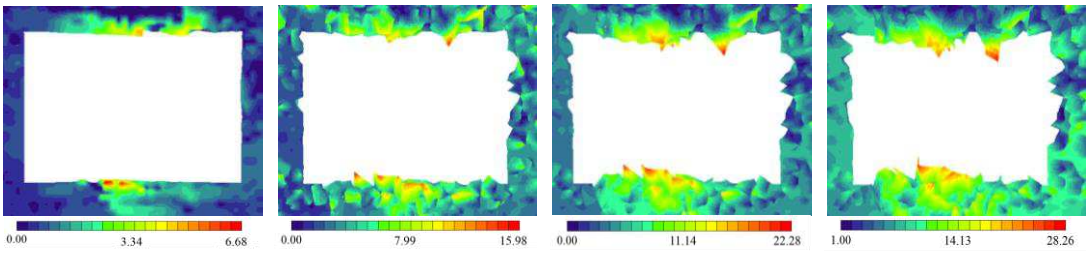

(a) 2000s (b) 8200s (c) 10800s (d) 12000s

Figure 11. Displacement field in scheme two.

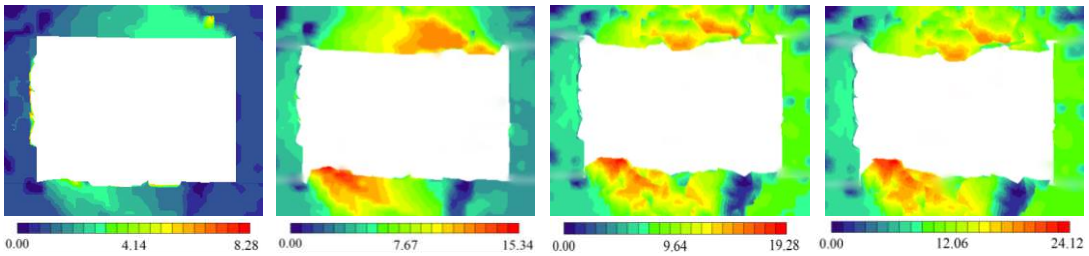

(a) 2200s (b) 5900s (c) 8800s (d) 14000s

Figure 12. Displacement field in scheme three.

It can been seen from **Fig. 10** that at 2200s after roadway excavation, the displacement of roof increases first, and the displacement is about 11mm. Slight roof caving occurred in the shallow bedding surface, a small amount of surrounding rock caving occurred, and there was no deformation and failure on both sides and floor of the roadway. At 7000s, the displacement of roof continues to increase, reaching 21mm, and caving failure occurs. At 7800s, the right side and the floor have a large displacement, the convergence of the roadway is significant., and the floor heave is about 17mm. At 9000s, the overall displacement of surrounding rock is large, and the displacement of roof, floor and right side is more than 30mm, resulting in serious damage of roadway. It can been see from **Fig. 11** that at 2000s after roadway excavation, the surrounding rock in the middle of the roof and floor has a large displacement of about 6mm, while the other surrounding rock has no obvious change. As the roadway was supported by the bolt, the surrounding rock and the bolt formed a bearing structure together, and the bearing capacity of the surrounding rock was improved. At this stage, the deformation of the surrounding rock showed complete deformation characteristics of the surrounding rock, and there was no significant deformation and no obvious fracture development, and the roadway was in a relatively stable state. At 8200s, the deep surrounding rock has a small displacement between 8mm and 16mm. At 10800s, the displacement of floor reaches 20mm, roof collapse occurs, floor heave occurs, and there is no obvious laminated damage on both sides. At 12000s, the displacement of floor and roof reached about 28mm, and serious deformation occurred. It can been see from **Fig. 12** that at 2200s after roadway excavation, the surrounding rock on the right side of roof and left side of floor has a small displacement of only 4mm. At 5900s, the displacement of the right side of the roof

and left side of the floor continued to increase, but the displacement of the left and right side of the roadway did not increase greatly. At 8800s, the floor heave of the bottom plate reaches 19mm. At 14000s, the surrounding rocks in the shallow and deep parts have a large displacement, and the displacement of the roof and floor of the roadway is the largest, reaching 24mm.

Figure 13 gives the comparison of roadway final displacement. In scheme one, the deformation of surrounding rock from large to small is the roof, floor and side. This indicates that the roof damage is the most serious after excavation, and obvious subsidence damage appears at the early stage of excavation, while the deformation of the floor and the side of the roadway is relatively slow, and the deformation rate gradually increases with the passage of time. In scheme two, the deformation of surrounding rock from large to small is the floor, roof and side. It shows that the bolt support can effectively control the deformation of the roof and the side, while the floor has the largest degree of damage and the fastest deformation due to the lack of support. In scheme three, the deformation of surrounding rock from large to small is the roof, floor and side. It shows that the combined support of bolt and anchor cable has obvious control effect on the roof and side, while the deformation of the floor without support is the fastest.

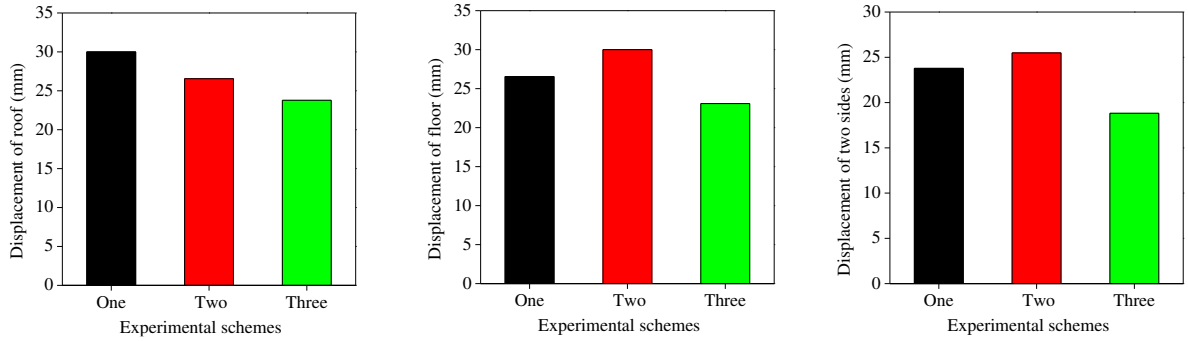

(a) Roof (b) Floor (c) Side

Figure 13. Comparison of roadway final displacement.

In addition, there are obvious differences in the deformation of surrounding rock with different support schemes. By comparison, the displacement of the roof decreases successively from scheme one to scheme three. The displacement of the roof in scheme one is 30mm, the displacement of the roof in scheme two is 26.55mm, which is reduced by 11.50% compared with that in scheme one. The displacement of the roof in scheme three is 23.78mm, which is reduced by 10.43% compared with that in scheme two. The floor displacement of both schemes one and two is influenced by the displacement meter range of 30mm, while the floor displacement of scheme three is 25.49mm, which is reduced by 15.03% compared with that of schemes one and two. The variation trend of the wall displacement is consistent with that of the roof, which still decreases successively from scheme one to scheme three. The wall displacement of scheme 1 is 30mm, the wall displacement of scheme two is 23.08mm, which is 23.07% less than that of scheme 1. The wall displacement of scheme three is 18.82mm, which is 18.42% less than that of scheme 2. In general, the displacement of different scheme of roadway size rule is: scheme one > scheme two > scheme three, without the support of roadway deformation is the most serious, and after using the roadway anchor supporting roadway convergence has been a certain degree of control, and USES the anchor rod and anchor rope support effect is better than a single bolt support, on the control effect is best.

3.2 Failure characteristic

Figure 14 shows the failure modes of roadway surrounding rock of different schemes. According to the process of deformation and failure as shown in **Figs. 10-12**, under the condition of no support, the failure of the layered surrounding rock of the roadway is gradual, and the surrounding rock has the characteristics of broken after broken, and then broken again. The internal deformation of the surrounding rock is mainly shear slip failure, while the surrounding rock of the roadway supported by bolt and anchor cable is mainly compression shear failure.

In scheme one, the tension effect of radial stress and tangential stress under the shearing action of resultant shear plane area shallow strata sliding deep extension to extension fracture in different point of view, lead to the strength of surrounding rock in roadway roof and floor and two low, poor stability, left and right sides of the formation of the cracks expanding, roof, roof surrounding rock with fracture, The caving

occurs under the weight effect, showing the characteristics of loose-type caving. This kind of caving mode is mainly caused by the gravity action of fractured rock mass, which shows a dynamic development process of gradually caving upward. The cracks generated on the two sides of the roadway continuously lead to the spalling of surrounding rock wall, thus forming a new free surface, driving the next round of deformation, and causing the failure to develop inwards. In Scheme two, since there is no anchor support for the roadway floor, the development of shear cracks is all within the floor range and continuously extends to the deep, and finally three shear slip lines are formed. There is an obvious of roof absciss layer, roof subsidence amount is larger, the right side of the roof rock damage further deepened, the serious of floor heave of roadway, floor rock mass was fully ejection and shallow and deep rock mass from the lower level of rock mass, two significant convergence phenomenon, but with the rock and the formation of the surrounding rock anchorage effect, the roadway makes some piece of help, The collapse failure of large area of roof surrounding rock is also the last of the test. Therefore, it can be seen that the anchor bolt mainly strengthens the shallow surrounding rock, combines the small rock mass in the broken zone into large rock mass through the anchoring effect, and forms the composite beam structure between the roof and surrounding rock in the roadway. In scheme three, the shear cracks in the roadway floor developed continuously because there was no support for the roadway floor, and finally three obvious shear slip lines were formed. Under the action of gravity of overlying rock mass and horizontal extrusion pressure, the roof of the roadway bent and sank as a whole without caving, indicating that the anchor cable suspended the composite beam structure formed in the deep more stable surrounding rock, giving full play to the role of deep surrounding rock. The two sides of the roadway have no obvious deformation and no sheet wall failure, indicating that the synergistic anchoring effect of anchor bolt and anchor cable is significant. However, due to the lack of support measures for the floor, the floor heave of the roadway was serious, and the layered rock mass on the left side of the floor was completely ejected.

(a) Scheme one (b) Scheme two (c) Scheme three

Figure 14. Failure form of surrounding rock in different support methods of similar test.

4. Discussion

4.1. Mechanism of roof instability of layered surrounding rock without support

From the physical test results, it can be seen that, compared with the intact enclosed rock mass, the ability of roadway layered surrounding rock to resist deformation is weaker, and its deformation and failure are more serious after roadway excavation. In particular, the layered roof without support is prone to bed separation and roof caving.

The excavation of roadway will cause the stress redistribution phenomenon in the surrounding rock, which will lead to the decrease of the unloading effect of the roof. Under the synergistic action of the dead weight stress and the horizontal stress, the mutual clamping effect between the layers of rock will gradually weaken, and finally lead to the bending and sinking of the layered rock mass of the roof. In the process of bending and sinking, the upper part of the layered rock mass of the roof is compressed in the horizontal direction, while the lower part is tensioned, resulting in the relative sliding between layers. The process was analyzed with the beam structure, and the instability phenomenon was analyzed with the second layer rock mass as the research object. As shown in Fig. 15, when the lower layer body bent and sank, the gravity of the lower layer body would generate tensile stress on the bedding plane of the upper layer.

The tensile stress can be obtained according to **Eq. (1):**

$$\sigma=\gamma H$$

Where γ is bulk density of rock mass, H is thickness of lower strata.

If $\sigma>\sigma_1$ (σ_1 is the tensile strength between bedding planes) and the bending stiffness of the lower strata is less than that of the upper strata, the bed separation phenomenon will occur and the roof will be unstable. Instead, the upper and lower layers bend and sink together as composite beams. If the upper and lower strata bend and sag together in the form of composite beams, but the shear strength of bedding plane is less than the shear stress between bedding planes, and the bending stiffness of the lower strata is less than that of the upper strata, the bed separation will occur and the roof will be unstable; otherwise, the bed separation will not occur and the roof will be stable.

Among them, the shear stress between bedding structural planes is:

$$\tau=\frac{Q}{2I_Z}\left(\frac{h^2}{4}-d^2\right) \tag{4}$$

Where Q is the shear force on the cross section, I_z is the moment of inertia of the section relative to the neutral axis, h is the sum of the thickness of the upper and lower strata, d is Distance from bedding plane to neutral axis.

The shear strength of the bedding plane meets the Mohr-Coulomb criterion:

$$\tau=c+\sigma\tan\theta \tag{5}$$

where τ is the shear stress, c is cohesive force, σ is the normal stress, θ is the angle of internal friction.

In layered roof surrounding rock, is apart from the roadway surface layer 1 of the stability of the worst recently, is also the most prone to bend subsidence, level 1 after bending failure from layer 2, layer 2 would become surface layer, its stress conditions are similar to 1 layer, if the bending failure conditions lead to upper rock layer 3 and into the surface layer and so on, Until the rock mass of a layer in the deep roof does not meet the failure conditions to reach the equilibrium, in this process, strata separation may occur between the layers of the roof, and the rock mass of each layer is destabilized one after another, finally leading to the overall instability of surrounding rock.

4.2. Mechanism of roof instability of layered surrounding rock with support

From the above content, without supporting of surrounding rock of roadway roof in lower level of low tensile and shear strength of layered rock mass is the source of instability of roadway bolt and anchor cable bolting and grouting methods, can strengthen the tensile and shear strength between the rock mass, and make the roof strata to form composite beams bearing structure as a whole.

In order to study the instability mechanism of the roadway roof in this case, the composite beam of the roof was taken as the research object for analysis, and the longitudinal unit length of the composite beam was taken, as shown in **Fig. 15**.

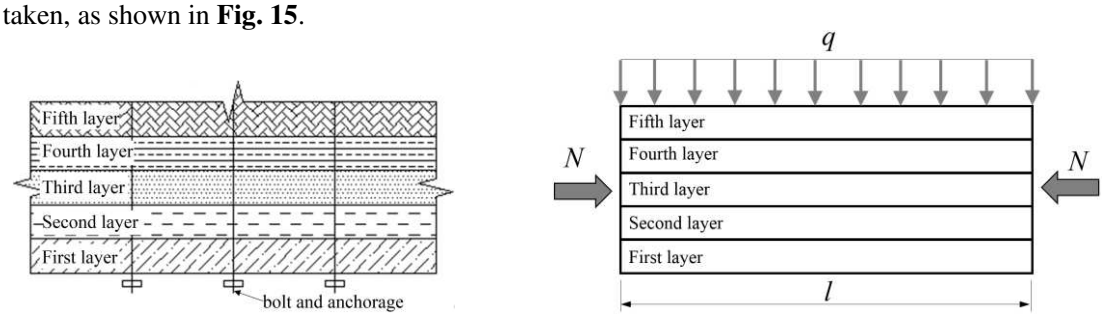

Figure 15. Composite beam structure in roof.

Under the action of gravity of overburden and horizontal lateral stress, the bending deformation equation of composite beam is:

$$D\frac{d^2W}{dx^2}=-M \tag{6}$$

$$D=\frac{Ed^3}{12\left(1-\nu^2\right)} \tag{7}$$

$$M = NW + \frac{1}{2}qlx - \frac{1}{2}qx^2 - \frac{ql^2}{12} \tag{8}$$

where q is gravity of overlying strata, N is horizontal lateral stress, W is deflection of composite roof beams in vertical direction, l is roadway width, d is thickness of roof composite beam, E is the equivalent modulus of elasticity,ν is the Equivalent Poisson's Ratio.

It is assumed that the thickness of each rock layer forming the composite beam is d_1, d_2, …, d_n the elastic modulus of each rock layer is respectively E_1, E_2, …, E_n, the Poisson's ratio of each rock layer is respectively v_1, v_2, …, v_n. Then the equivalent elastic modulus and equivalent Poisson's ratio of the composite beam are:

$$\left.\begin{aligned} E{=}E_1\frac{d_1}{d} + E_2\frac{d_2}{d} + \mathrm{L} + E_i\frac{d_i}{d} = \sum_{i=1}^{n} E_i\frac{d_i}{d} \\ \nu{=}\nu_1\frac{d_1}{d} + \nu_2\frac{d_2}{d} + \mathrm{L} + \nu_i\frac{d_i}{d} = \sum_{i=1}^{n} \nu_i\frac{d_i}{d} \end{aligned}\right\} \tag{9}$$

According to **Eq. (6)**, it can be obtained:

$$W = A\cos kx + B\sin kx + \frac{q}{2N}\left(x^2 - lx + \frac{l^2}{b} - \frac{2}{k^2}\right) \tag{10}$$

In the formula:

$$k^2 = \frac{N}{D} \tag{11}$$

The boundary conditions of **Eq. (10)** are as follows:

$$W(x)\Big|_{\substack{x=0\\x=l}} = 0 \tag{12}$$

From **Eqs. (10)**-**(12)**, we can get:

$$W{=}\frac{q}{N}\left\{\left(\frac{1}{k^2} - \frac{l^2}{12}\right)\left(\cos kx + \tan\left(\frac{kl}{2}\right)\sin kx\right) + \frac{x^2}{2} - \frac{lx}{2} + \frac{l^2}{l^2} - \frac{1}{k^2}\right\} \tag{13}$$

Considering symmetry, the deflection of the beam plate is maximized at $x = \frac{l}{2}$:

$$W_{\max}{=}\frac{q}{Nk^2}\left[\left(1 - \frac{k^2l^2}{12}\right)\sec\left(\frac{kl}{2}\right) - \left(1 + \frac{k^2l^2}{24}\right)\right] \tag{14}$$

If $W_{\max}$ is infinite, it should satisfy:

$$\frac{kl}{2}{=}\frac{n\pi}{2}\left(n = 1,3,5\mathrm{L}\ \mathrm{L}\right) \tag{15}$$

Then k is:

$$k{=}\frac{n\pi}{l}\left(n = 1,3,5\mathrm{L}\ \mathrm{L}\right) \tag{16}$$

According to **Eqs. (11)** and **(16)**,

$$N{=}\left(\frac{n\pi}{l}\right)^2 D \tag{17}$$

In **Eq. (17)**, when n=1, the minimum critical value N_{min} is:

$$N_{\min}{=}\left(\frac{\pi}{l}\right)D \tag{18}$$

According to **Eqs. (15), (17)** and **(18)**, we can get:

$$\left.\begin{aligned} n^2 &= \frac{N}{N_{\min}} \\ \frac{kl}{2} &= \frac{\pi}{2}\sqrt{\frac{N}{N_{\min}}} \end{aligned}\right\} \tag{19}$$

Substituting **Eq. (19)** into **Eq. (14)**, we can obtain:

$$\frac{W_{\max}}{\overline{W}} = \left(\frac{N_{\min}}{N}\right)^2 \left[\left(1-\frac{\pi^2 N}{12N_{\min}}\right)\sec\frac{\pi}{2}\sqrt{\frac{N}{N_{\min}}} - \left(1+\frac{\pi^2 N}{24N_{\min}}\right)\right] \tag{20}$$

In the **Eq. (20)**:

$$\overline{W} = \frac{ql^4}{\pi^4 D} \tag{21}$$

According to **Eq. (20)**, the relation between $\frac{W_{\max}}{\overline{W}}$ and $\frac{N}{N_{\min}}$ can be obtained, and the stress conditions of the composite beam structure of the roadway roof when bending and fracture occur can be obtained as follows:

$$N \geq 0.7N_{\min} \tag{22}$$

Assume that the average bulk density of overlying strata in the roadway is γ and the buried depth of the roadway is H. Through **Eqs. (7), (18)** and **(22)**, we can get:

$$\lambda\gamma H \times d \times 1 \geq \frac{\pi^2 E d^3}{16l^2\left(1-v^2\right)} \tag{23}$$

where λ is horizontal lateral stress coefficient.

By simplifying **Eq. (23)**, the basic mechanical conditions for the instability of composite roof beams can be obtained as follows:

$$\lambda\gamma H \times d \geq \frac{\pi^2 E}{16i^2\left(1-v^2\right)} \tag{24}$$

where *I* is the span thickness ratio of composite roof beams.

$$i = \frac{l}{d} \tag{25}$$

Assuming that the other parameters are certain, the critical span thickness ratio for bending failure of composite roof beams can be obtained from **Eq. (26)** as follows:

$$i_{cr} = \frac{\pi}{4\sqrt{\frac{1-v^2}{E}\times\lambda\gamma H}} \tag{26}$$

In scheme two and three, however, still appear the abscission layer phenomenon, mainly because of roof rock combination by gravity stress and horizontal ground stress, anchorage zone can't bear the vertical direction of the cavern roof extrusion and cannot prevent fracture caused by horizontal tensile stress, the bending deformation of anchorage zone, roof in the roof bedding shear failure happened to the weak surface level, The local stress concentration at the end of the anchor bolt group further intensifies the separation of the weak plane of bedding, and the anchorage area continues to deform and destroy until the whole collapse and the bedding separation is generated. Therefore, according to the geological conditions

of this test and combined with the failure types of roadway roof in the test process, the type of roof caving in scheme two and scheme three is extrusion caving, and the roof caving is mainly caused by the shear effect of secondary horizontal stress on the roof. It can be seen that the axial force provided by the anchor bolt and cable can restrain the separation between layered rock masses and effectively increase the friction between rock strata. The anchor bolt and cable itself can also provide a certain shearing capacity to restrain the relative sliding between rock strata, enhance the bearing capacity of surrounding rock and the ability to control the separation and horizontal dislocation of the roof.

5. Conclusions

In this paper, based on the deep roadway and surrounding rock conditions of 742m~877m in eastern China, the physical model test of layered surrounding rock of rectangular roadway under three different support modes from excavation to instability failure is carried out by using the self-developed two-dimensional physical model test system of underground engineering. The whole process of model failure was monitored by means of digital speckle technique. The main conclusions are as follows:

(1) The results of digital speckle show that the convergent displacement of roadway surface in different schemes is in the order of scheme 1, scheme 2 and scheme 3. The surrounding rock displacement of the roadway without support is the largest, and the maximum displacement value at the time of final failure is 38.18mm. The surrounding rock displacement of the roadway supported by bolt and anchor cable is the smallest, and the maximum displacement value at the time of final failure is 24.12mm. The tunnel failure time of Scheme 1 is the fastest and 9000s, and the tunnel failure time of Scheme 3 is 14000s, 55.56% more than that of Scheme 1. In the second and third schemes, the anchor bolt and the shallow layered surrounding rock form the composite beam bearing structure, which has a certain control effect on the deformation of surrounding rock.

(2) Different schemes have different failure types and instability mechanisms of roadway. In scheme 1, the surrounding rock is mainly damaged by shear slip, and the caving type is loose-type caving, and the instability mechanism type is weak-surface control. The concrete failure characteristics are as follows: the roof surrounding rock caving in a large area, and the slabs and floor heave are serious. Plan two, three pressure on shear failure and shearing slip damage of surrounding rock is given priority to, catastrophic collapse types for JiYaXing catastrophic collapse, the instability mechanism of the type of strength - stress control type, the former part of roof rock caving, a little help, floor heave is serious, while the latter is only a little caving of roof rock, no help phenomenon, only going to see a slight bottom floor drum.

(3) The tensile and shear resistance of laminated roof surrounding rock is weak. In the absence of support, the laminated roof surrounding rock is easily separated from each other at the bedding plane, resulting in bending deformation and bed separation. After adopting effective support, the laminated roof surrounding rock is transformed into a composite beam bearing structure, and the stability of surrounding rock increases. By comparison with the failure modes of roadway under different support way, bolts or cables to a certain extent, can control the damage of the surrounding rock deformation, control the deformation of broken continues to develop, to loose and broken area within the scope of the surrounding rock control function, and improve the stress state of surrounding rock, which have played an important role in stability of surrounding rock of roadway.

Acknowledgements

This work was supported by National Natural Science Foundation of China (51734009, 52074259). The authors gratefully appreciate these supports.

References

Amodio, D.; Broggiato, G.B.; Campana, F.; Newaz, G.M. Digital speckle correlation for strain measurement by image analysis. *Exp. Mech*. **2003**, *43(4)*, 396–402.

Asadi, M.; Bagheripour, M.H.; Eftekhari, M. Development of optimal fuzzy models for predicting the strength of intact rocks. *Comput. Geosci-UK.* **2013**, *54*, 107–112.

Bewick, R.P.; Kaiser, P.K.; Amann, E. Strength of massive to moderately jointed hard rock masses. *J Rock Mech. Geotech.* **2019**, *11(3)*, 562–575.

Bruck, H.A; Mcneill, S.R.; Sutton, M.A.; Peters, W.H. Digital image correlation using Newton-Raphson method of partial differential correction. *Exp. Mech*. **1989**, *29(3)*, 261–267.

Ding, X.L.; Niu, X.Q.; Pei, Q.T.; Huang, S.L.; Zhang, Y.T.; Zhang, C.H. Stability of large underground caverns excavated in layered rock masses with steep dip angles: A case study. *B. Eng. Geol. Environ.* **2019**, *78(7)*, 5101–5133.

Do, N.A.; Dias, D.; Dinh, V.D.; Tran, T.T.; Dao, V.C.; Dao, V.D.; Nguyen P.N. Behavior of noncircular tunnels excavated in stratified rock masses-Case of underground coal mines. *J. Rock Mech. Geotech.* **2019**, *11(1)*, 99–110.

Feng, X.T.; Pei, S.F.; Jiang, Q.; Zhou, Y.Y.; Li, S.J.; Yao, Z.B. Deep fracturing of the hard rock surrounding a large underground cavern subjected to high geostress: In situ observation and mechanism analysis. *Rock Mech. Rock Eng.* **2017**, *50(8)*, 2155–2175.

Halakatevakis, N.; Sofianos, A.I. Correlation of the Hoek-Brown failure criterion for a sparsely jointed rock mass with an extended plane of weakness theory. *Int. J. Rock Mech. Min.* **2010**, *47(7)*, 1166–1179.

Li, Y.H.; Tang, X.J.; Yang, S.; Chen, J.W. Evolution of the broken rock zone in the mixed ground tunnel based on the DSCM. *Tunn. Undergr. Sp. Tech.*. **2019**, *84*, 248–258.

Lyu, C.; Zeng, Z.Q.; Dong, Y. Limit analysis of progressive asymmetrical collapse failure of tunnels in inclined rock stratum. *Symmetry-Basel* **2019**, *11(7)*, 904.

Lyu H.M.; Shen S.L.; Zhou A.; Chen K.L. Calculation of pressure on the shallow-buried twin-tunnel in layered strata. *Tunn. Undergr. Sp. Tech.* **2020**, *103*, 103465.

Xu, D.P.; Feng, X.T.; Chen, D.F.; Zhang, C.Q.; Fan, Q.X. Constitutive representation and damage degree index for the layered rock mass excavation response in underground openings. *Tunn. Undergr. Sp. Tech.* **2017**, *64*, 133–145.

Yang, S.; Li, Y.H.; Chen, M.; Liu, J.S. Incompatible deformation and damage evolution of mixed strata specimens containing a circular hole. *Geomech. Eng.* **2020**, *20(5)*, 461–474.

Yang, X.X.; Kulatilake, P. H. S. W; Jing, H.W.; Yang, S.Q. Numerical simulation of a jointed rock block mechanical behavior adjacent to an underground excavation and comparison with physical model test results. *Tunn. Undergr. Sp. Tech.*. **2015**, *50*, 129–142.

Yoshinaka, R.; Osada, M.; Park, H.; Sasaki, T.; Sasaki, K.. Practical determination of mechanical design parameters of intact rock considering scale effect. *Eng. Geol.* **2008**, *96(3-4)*, 173–186.

Zhao S.; Zhang D.M.; Huang H.W. Deep learning–based image instance segmentation for moisture marks of shield tunnel lining. *Tunn. Undergr. Space Technol.* **2020**, *95*, 103156.

Zhou, H; Song, M; Zhang, C.Q.; Hu, D.W.; Lu, J.J. Physical model tests of the surrounding rock deformation and fracture mechanism of mixed-face ground under TBM tunneling. Eur. J. Environ. Civ. En. **2020**, *24(11)*, 1744–1760.

Zhou, Y.Y.; Feng, X.T.; Xu, D.P.; Fan, Q.X. An enhanced equivalent continuum model for layered rock mass incorporating bedding structure and stress dependence. *Int. J. Rock Mech. Min.*. **2017**, *97*, 75–98.